



Properties optimization of electrospun polymer: organic-free perovskite nanofibers by controlling solution concentration

Muhammad A. Bkkar¹ · Roman O. Olekhovich² · Arina V. Kremleva³ · Vera E. Sitnikova¹ · Yakov N. Kovach³ · Nikolai A. Zverkov⁴ · Mayya V. Uspenskaya¹

Received: 21 February 2023 / Accepted: 20 April 2023 / Published online: 11 May 2023
© The Polymer Society, Taipei 2023

Abstract

In this paper, properties of electrospun polyvinylpyrrolidone-cesium lead iodide (CsPbI₃) nanofibers have been optimized by controlling the solution concentration. The diameter of nanofibers was found to enlarge from 215 to 558 nm with increasing polymer concentration and to decrease from 481 to 228 nm with reducing total material concentration. The solution concentration was employed to alter the polymer structural confinement and organic-free perovskite stability to obtain maximum perovskite crystallinity and improved optical properties at a polymer to perovskite ratio of 15% and a material concentration of 43%. The results showed that with an increase in polymer concentration or a decrease in material concentration, the shrinkage ratio increases in the range of 13–20%, and higher tensile properties are achieved with strain of 2.5–3.5% and tensile strength of 1.4–1.9 MPa. The added perovskite significantly reduces the shrinkage ratio, which increases from 12–14% to 28–31% by decreasing perovskite concentration from 45 to 35%. Defects related to shrinkage can be eliminated by enhancing the nanofibers' adherence to the substrate, using substrates with a higher Young's modulus than the nanofibers, and reducing the thickness of the nanofibers. The resulting nanofibers showed high thermal stability with a weight loss of 1.8% to 3.6% at a temperature of 200 °C.

Keywords Polymer · Perovskite · Nanofibers · Concentration · Diameter · Properties

✉ Muhammad A. Bkkar
mbkkar@itmo.ru

Roman O. Olekhovich
r.o.olekhovich@mail.ru

Arina V. Kremleva
avkremleva@itmo.ru

Vera E. Sitnikova
v.e.sitnikova@gmail.com

Yakov N. Kovach
yakovachyakov@gmail.com

Nikolai A. Zverkov
nikolai.zverkov@metalab.ifmo.ru

Mayya V. Uspenskaya
mv_ustpenskaya@itmo.ru

¹ Chemical Engineering Center, ITMO University, Saint-Petersburg 197101, Russia

² Faculty of Control Systems and Robotics, ITMO University, Saint-Petersburg 197101, Russia

³ Institute of Advanced Data Transfer System, ITMO University, Saint-Petersburg 197101, Russia

⁴ Department of Physics, ITMO University, 197101 Saint-Petersburg, Russia

Introduction

Recently, electrospun polymer–perovskite nanofibers have become a popular area of research to fabricate diverse optoelectronic devices owing to their low cost and unique properties [1–4]. The generally utilized method for fabricating these nanofibers is the one-stage electrospinning method, which is fast, simple, and inexpensive [2, 5–7]. To increase the optoelectronic device performance, improving the nanofibers properties is considered crucial [2, 5, 6]. Their properties can be influenced by several factors, related to the setup of the electrospinning process [5, 8, 9], the environment [10], and the solution, i.e., the perovskite [7, 11, 12] and polymer [2, 5–7, 11] used and their concentration. The electrospinning setup (e.g., electrical voltage and collector type) can impact the orientation, tensile properties of nanofibers, and perovskite crystallinity [5, 8, 9]. The environmental conditions (i.e., temperature and humidity) can control the rate of solvent evaporation and affect the arrangement of the intermediate phase [10]. The type of perovskite (e.g., CsPbI₃ or MAPbI₃) can influence annealing conditions, perovskite crystallinity, optical properties, and thermal stability [3, 7, 11, 12]. The

type of polymer, e.g., polyvinylpyrrolidone (PVP), polyacrylonitrile (PAN), or polyvinyl alcohol (PVA), can determine the thermal behavior and tensile properties of nanofibers [5, 7, 9, 11]. After electrospinning, the polymer can form an intermediate phase with perovskite precursors, promoting perovskite nucleation, which is further stabilized by the polymer after annealing [5, 6, 9, 13]. Changes in the solution concentration (i.e., polymer or perovskite concentration) can highly influence the nanofibers average diameter and therefore change the diameter-related properties [5, 6, 14]. Some studies have explored the impact of electrospinning solution concentration on the properties of one-stage electrospun polymer-MAPbI₃ nanofibers. Li et al. [7] and Meng et al. [11] studied influence of perovskite concentration on properties of MAPbI₃:PAN and MAPbX₃:PVA nanofibers, respectively. They discovered that increasing perovskite concentration makes the surface of nanofibers rougher, and the average diameter with well-dispersed perovskite nanocrystals increases. The crystallinity of perovskite and optical properties improve with increasing perovskite concentration. Bohr et al. [6] investigated the impact of the PVP/MAPbI₃ ratio on the morphology and crystallinity of nanofibers. They found that the nanofibers average diameter increases and perovskite crystallinity diminishes with increasing the polymer concentration. Chen et al. [14] considered the impact of PVP content on the morphology of nanofibers and the distribution regions of MAPbI₃ nanocrystals within the nanofiber structure. The results showed that at low polymer concentrations, the nanocrystals are located near the center and surface of the nanofibers. An increase in polymer concentration causes the surface of the nanofibers to become smoother, and nanocrystals are observed only in their core. Prior studies have lacked data on the shrinkage ratio and tensile properties. Furthermore, polymer-MAPbI₃ nanofibers have a low operating temperature due to the low phase transition temperature (54–57 °C) of MAPbI₃ used. Whereas the operating temperature of solar conversion devices is higher, for example, it is ~80 °C for solar cells [6, 15, 16]. Organic-free CsPbI₃ perovskite is considered an optimal alternative to MAPbI₃ because of its high thermal stability, the wide light absorption spectrum up to 700 nm, and the long diffusion length of charge carriers [17–20]. However, preparation of nanofibers modified with CsPbI₃ nanocrystals is considered a major challenge due to the required high annealing temperature (> 300 °C) [21, 22] and the low solubility of CsI [23, 24]. Polymers should have sufficient thermal stability and chemical compatibility with perovskite precursors. In our previous works [5, 9], organic-free CsPbI₃ nanocrystals-modified PVP nanofibers were successfully obtained, and the effect of setup parameters on their properties was determined. In this paper, for the first time, the effect of solution concentration on the properties (i.e., morphology, crystallinity, optical properties, shrinkage ratio, tensile properties, and thermal stability) of PVP:CsPbI₃ nanofibers fabricated by a one-stage electrospinning method was studied. The polymer concentration was changed from 7.5% to 15%, and then the

concentration of total material (i.e., perovskite and polymer) was decreased from 49 to 38% to find the optimal solution concentration that leads to the fabrication of high-quality nanofibers.

Materials and methods

The study's methodology and materials are similar to those utilized in our prior publications [5, 9].

Materials

99.5% pure lead (II) iodide (PbI₂) and 99.9% pure cesium iodide (CsI) were received from Chemcraft in Russia. Additionally, Sigma-Aldrich in Germany provided anhydrous dimethylformamide (DMF) with 99.8% purity and PVP with a molecular weight of ~1,300,000.

Preparation methods

Electrospinning solutions

To make the PVP solution, the polymer was dissolved in DMF for 5 min at 300 rpm using magnetic stirring. Then, perovskite precursors CsI and PbI₂ were added to the PVP solution in a molar ratio of 1:1. (Fig. 1a). The polymer concentration was changed from 7.5% to 15% (polymer to perovskite ratio: 9–18%), and then the concentration of total material was changed from 49 to 38% (polymer to perovskite ratio: 15%) (Fig. 1b). To achieve homogeneity, the solutions were stirred at 600 rpm for 60 min at 27 °C and 21% humidity.

Electrospun nanofibers

Nanofibers were fabricated using a one-stage electrospinning process and subsequently annealed in a laboratory oven for five minutes at 200 °C. Figure 1a depicts this procedure. The electrospinning solution, which was put into a 5 mL syringe, was processed using a Nanon 01A electrospinning machine. Under ambient conditions, nanofibers were collected using both planar and rotational collectors.

Cleaning substrates

The cleaning process of the substrates involved immersing them in an ultrasonic bath (UZV7/100-TH) at a temperature of 40 °C and a frequency of 22 kHz. Cleaning solutions

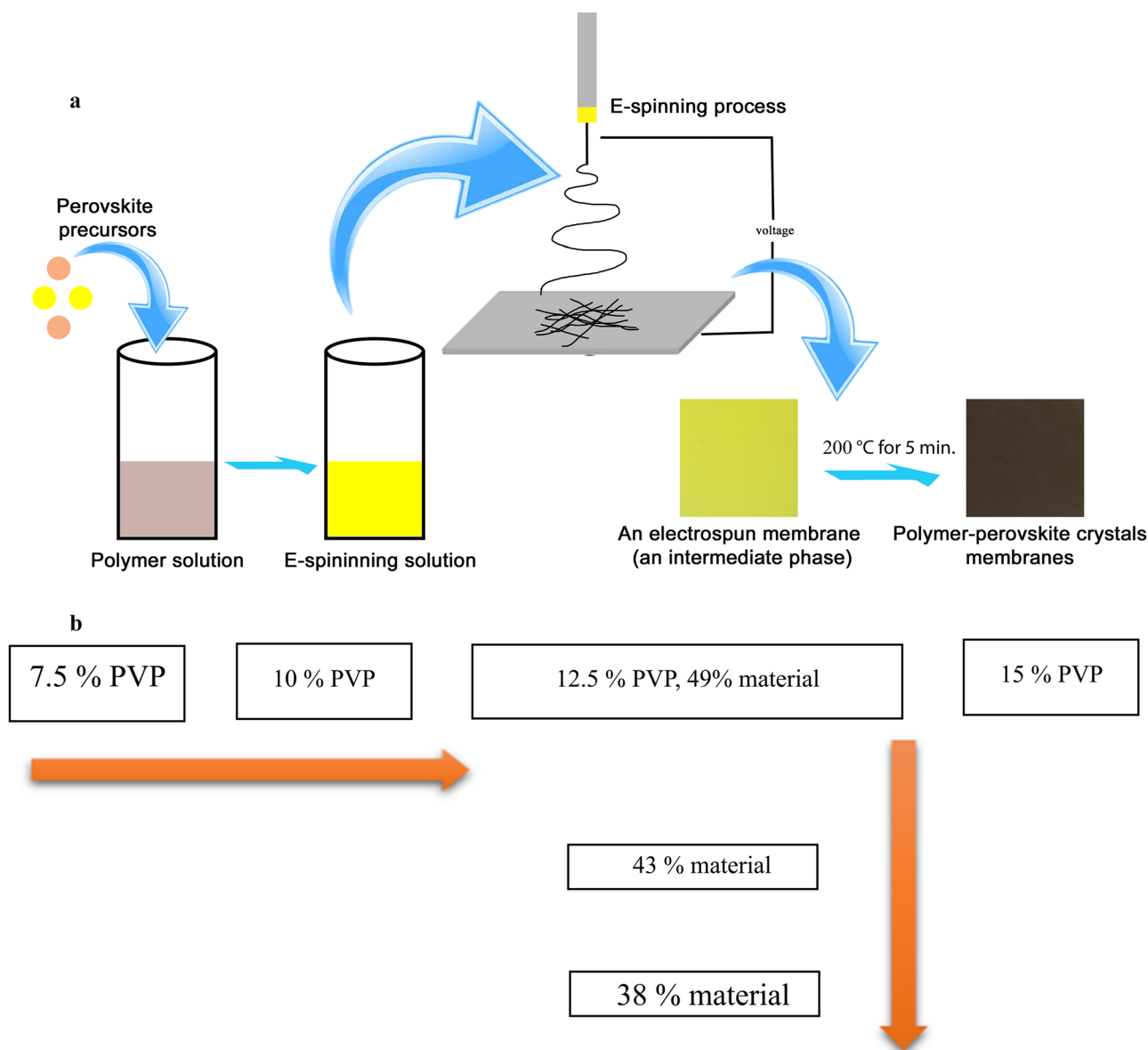


Fig. 1 Experimental steps: **a** from electrospinning solution to annealed nanofibers; **b** electrospinning solution concentration variation

such as water, acetone, and isopropanol were used, with each solution taking 25 min to clean. Following the cleaning process, the substrates were dried at a temperature of 200 °C for two hours in an oven.

Characterization methods

Morphology of nanofibers

First, nanofibers were prepared using the following electrospinning setup parameters: a voltage of 20 kV, a distance of 150 mm, a needle diameter of 0.42 mm, and a feed rate of 0.1 ml/h with a planar collector. Then, scanning

electron microscopy (SEM) images were acquired to describe the appearance of nanofibers and determine the average diameter using Image J software. The latter was found by measuring ~400 nanofibers from eight distinct places and averaging them.

Crystallinity

The nanofibrillar samples were fabricated utilizing the following electrospinning setup parameters: a voltage of 20 kV, a distance of 150 mm, a needle diameter of 0.42 mm, a feed rate of 0.1 ml/h, and a planar collector. X-ray diffraction (XRD) and differential scanning

calorimetry (DSC) were used to determine the crystallinity of samples. A DRON-8 X-ray device outfitted with a NaI (Tl) scintillation detector and a β -filter (Ni) was used to obtain XRD patterns. Meanwhile, DSC experiments were conducted in a nitrogen environment using a DSC 204 NETZSCH equipment with a 50 mL/min flow rate, a temperature range of 25–350 °C, and a heating rate of 10 K/min. The average of the three tests performed on each sample yielded the findings.

Optical properties

The nanofibrillar samples were prepared utilizing the following electrospinning setup parameters: a voltage of 20 kV, a distance of 150 mm, a needle diameter of 0.42 mm, a feed rate of 0.1 ml/h, and a planar collector. The optical properties were explored using spectra of light absorption and photoluminescence (PL). To acquire the light absorption spectra, a spectrometer system comprised of a photonic multichannel analyzer (PMA-12, Hamamatsu) and an integrating sphere (Everfine, 0.5 m) with a multi-photometer (Photo-2000Z) was employed. The PL spectra were recorded using an Agilent Cary Eclipse spectrofluorometer.

The shrinkage ratio

Electrospinning was used to prepare ten strips of nanofibers for each solution concentration using the following setup parameters: a voltage of 20 kV, a distance of 150 mm, a needle diameter of 0.72 mm, and a feed rate of 0.3 ml/h. The nanofibers were collected using a rotating collector at a speed of 500 rpm, and each strip was 10 cm long and 1 cm wide. Samples were cut in the both directions of the rotary collector (i.e., longitudinal (LD) and transverse (TD) directions). To calculate the ratio of shrinkage, the lengths of samples were measured before and after annealing. The shrinkage ratio was estimated by dividing the change in the length after annealing by the starting length before annealing and obtaining an average value.

Tensile properties

Electrospinning was used to prepare ten strips of nanofibers using the following parameters: a voltage of 20 kV, a distance of 150 mm, a needle diameter of 0.72 mm, and a feed rate of 0.3 ml/h. The nanofibers were collected using a rotating collector at a speed of 500 rpm, and each strip was 10 cm long and 1 cm wide. Samples were cut in the both directions of the rotary collector (longitudinal (LD) and transverse (TD) directions). An Instron 5943 was used at room temperature to determine the tensile properties of nanofibers. The test speed was set to one millimeter per minute, and the average results were calculated from 5 samples.

Thermal stability

The nanofibers were prepared at the following electrospinning parameters: a voltage of 20 kV, a distance of 150 mm, a needle diameter of 0.42 mm, a feed rate of 0.1 ml/h, and a planar collector. To analyze the thermal stability of nanofibers, thermogravimetric analysis (TGA) was conducted using a TG 209 F1 Libra instrument from NETZSCH. The analysis was performed under a nitrogen atmosphere with a 50 mL/min flow rate, and the temperature range was set from 25 °C to 475 °C with a heating rate of 10 K/min.

Results and discussion

Morphology of nanofibers

The impact of solution concentration on the annealed nanofibers morphology was studied using SEM images. The fabrication parameters of samples 1–6 are listed in Table 1. Figure 2 demonstrates how the appearance of nanofibers changes with solution concentration. SEM images are accompanied by illustrations that show the

Table 1 Fabrication parameters of samples 1–6

Sample Number	Polymer in DMF, w%	Perovskite in DMF, w%	Material in DMF, w%	Polymer to perovskite ratio, w%	Average diameter, nm
1	7.5	45.0	47.4–49.9	9.0	215 ± 70
2	10.0			11.9	353 ± 100
3	12.5			14.8	481 ± 122
4	15.0			17.7	558 ± 160
3 (ref.)	12.5–8.4	45.0	49.0	14.8	481 ± 122
5		39.1	43.0		329 ± 70
6		34.6	38.3		228 ± 51

nanofibers structure. Nanofibers with PVP concentrations of 7.5% to 10% have a core nanofibrillar structure decorated with nanowires. At a PVP concentration of 12.5–15%, the nanofibers have a main nanofibrillar structure covered with small, fluffy-like nanowires. No changes are observed in the original structure of the nanofibers with changes in material

concentration. Some split nanofibers are visible in Fig. 2a, which is attributed to the annealing process and the high proportion of perovskite into nanofibers, making them less flexible [9]. Table 1 presents the average diameter values of nanofibers after annealing with different solution concentrations. The average diameter increases from 251 to 571 nm as

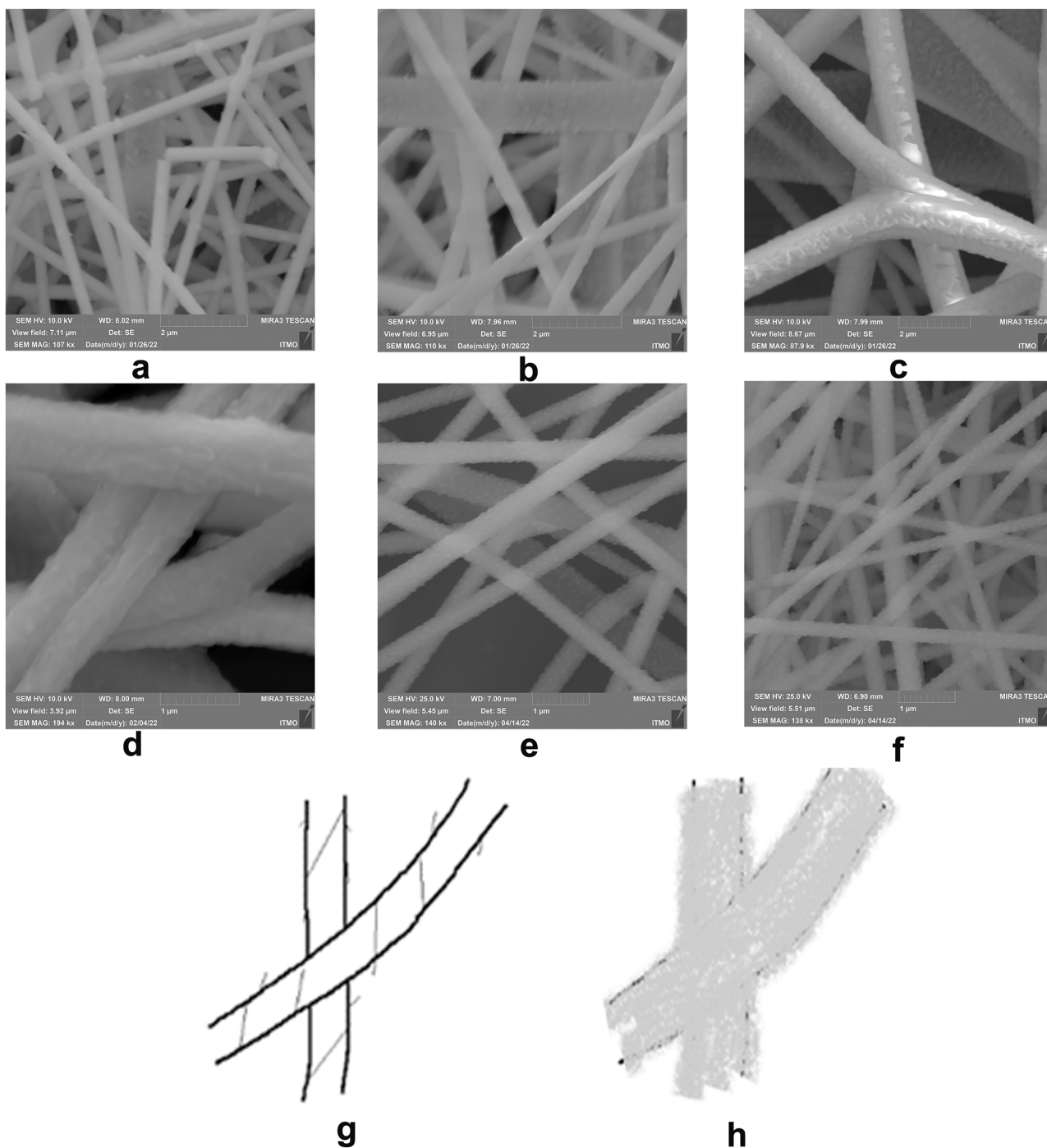


Fig. 2 Morphology of annealed nanofibers: **a** sample 1; **b** sample 2; **c** sample 3; **d** sample 4; **e** sample 5; **f** sample 6. A schematic illustration of the nanofibrillar structure: **g** samples (1–2); **h** samples (3–6)

the concentration of PVP increases from 7.5% to 15%. On the other hand, when the concentration of the total material is decreased from 49 to 38%, the average diameter decreases from 571 to 228 nm. The uniformity in the diameter worsens with increasing polymer concentration, while it improves with a decrease in material concentration.

Crystallinity

XRD and DSC were used to investigate the crystallinity. The XRD results, shown in Fig. 3a, confirm the PVP amorphous nature. The peaks at 14° , 20° , and 29° demonstrate the formation of perovskite crystals into polymer nanofibers, and the increase in their intensity indicates an improvement in the crystallinity (crystal size) [5, 9, 25]. After electrospinning, a complex (i.e., an intermediate phase) is formed between PVP and perovskite precursors,

lowering the annealing temperature necessary to obtain crystalline CsPbI_3 [5, 9, 25, 26]. XRD patterns show that the crystallinity of perovskite increases with an increase in PVP concentration from 7.5% to 12.5%, then decreases when PVP concentration reaches 15%. These findings can be explained by the dual effect of the polymer: stability and confinement effects. The perovskite crystals stability at room temperature improves with increasing polymer concentration; thus, XRD shows an increase in the crystallinity. However, at a high polymer concentration (15%), PVP into nanofibers limits the growth of crystals due to the confinement effect and the reduced mobility of perovskite precursors [6, 14]. Thus, as material concentration decreases while maintaining the polymer to perovskite ratio at 15%, the crystallinity of perovskite increases at 43% material concentration, then decreases slightly with a further decrease in material concentration. The decrease in material concentration reduces the confinement effect

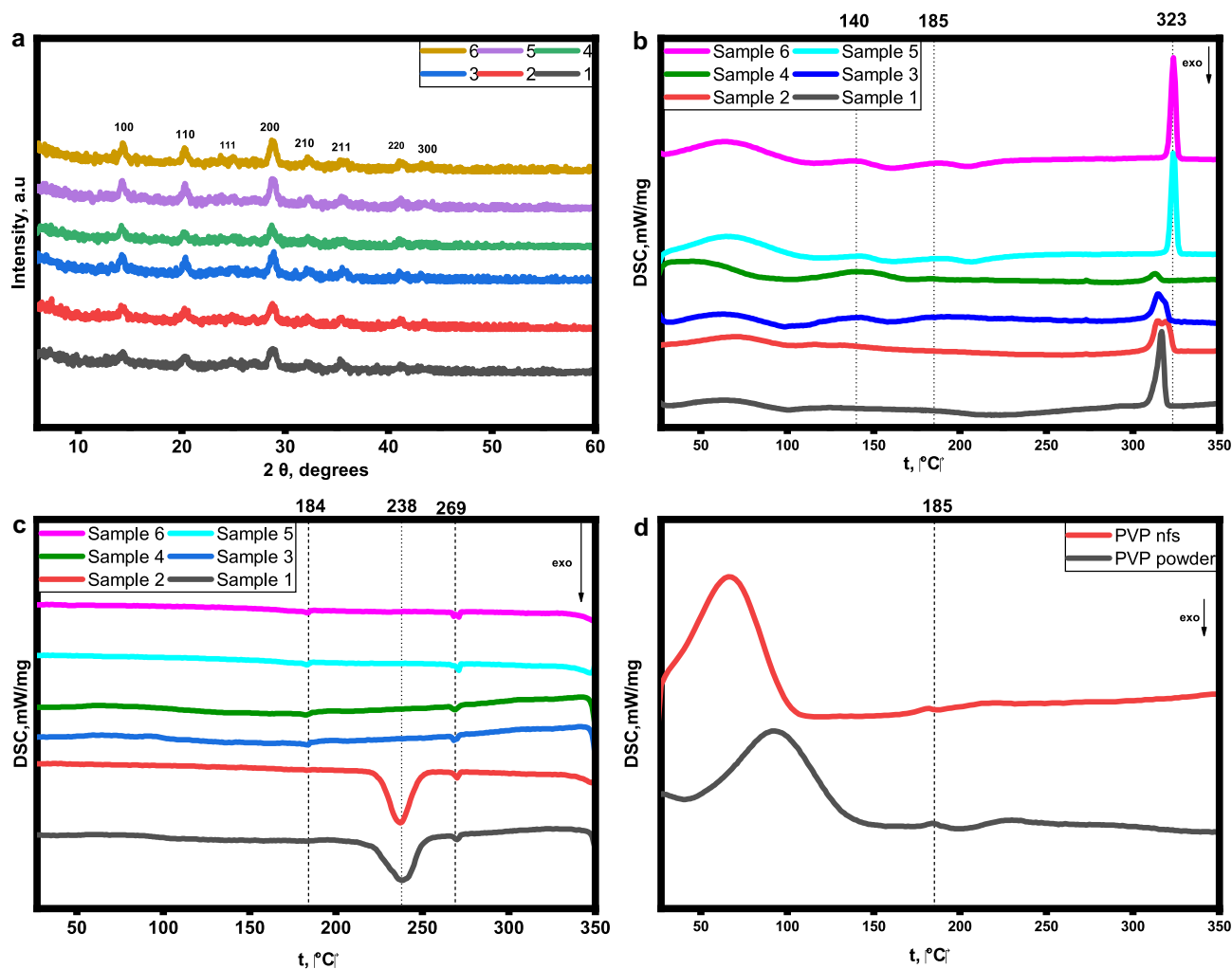


Fig. 3 Crystallinity results. **a** XRD patterns of samples (1–6); **b** DSC diagrams (heating cycles) of samples (1–6); **c** DSC diagrams (cooling cycles) of samples (1–6); **d** DSC diagrams of PVP powder and PVP nanofibers

Table 2 DSC results (heating cycles)

	Perovskite phase transition	Polymer–glass transition	α -CsPbI ₃ formation		
	T ₁ , °C (midpoint)	T ₂ , °C (midpoint)	T ₃ , °C (peak center)	ΔH_3 , J/g	*Crystallinity, %
PVP powder	–	179.9 ± 0.2	–	–	–
PVP nanofibers	–	175.5 ± 0.5	–	–	–
1	115.7 ± 4	–	316.3 ± 1.3	16.5 ± 1.3	84.4 ± 6.6
2	111.5 ± 1.5	–	314.5 ± 0.1 319.1 ± 0.2	16.4 ± 1.1	83.8 ± 5.6
3	121.0 ± 2.9	174.1 ± 1.6	314.4 ± 0.5	8.8 ± 2.6	45.0 ± 13.3
4	123.4 ± 1.1	179.7 ± 1.6	313.4 ± 0.8	4.7 ± 2.2	24.0 ± 11.2
5	129.1 ± 2.8	174.3 ± 0.2	322.3 ± 0.5	16.4 ± 0.1	83.8 ± 0.5
6	124.3 ± 3.8	175.1 ± 0.4	322.9 ± 0.3	15.4 ± 0.3	78.7 ± 1.5

*Crystallinity, % = $\Delta H_3 \times 100 / \Delta H_f$, $\Delta H_f = 19.56$ J/g [27]

of the polymer and increases the mobility of perovskite precursors, allowing larger crystals to form. However, a high decrease in material concentration can lower the stability of crystals at room temperature due to the high decrease in the nanofibers average diameter [5, 9], and thus, XRD indicates a decrease in the crystallinity. The crystallinity was further explored using DSC analysis, which confirmed the previous XRD results. The results are displayed in Fig. 3b–d, Tables 2 and 3. The DSC analysis reveals an endothermic peak around the temperature of 61 °C, which is related to dehydration. Another endothermic peak around the temperature of 140 °C could be associated with the formation of the perovskite crystalline phase, the reorganization of an intermediate phase, and/or the full evaporation of solvent residues [9]. The endothermic peak around the temperature of 185 °C is related to the glass transition of PVP [9]. The results showed that the polymer is amorphous, and the polymer T_g in the composite nanofibers is lower compared to PVP powder or PVP nanofibers due to the presence of perovskite, which increases the free volume between polymer chains. However, with an increase in polymer concentration, T_g increases. A small increase in T_g is observed by decreasing material concentration. The endothermic peak observed around the temperature of 323 °C is related to

the formation of cubic α -CsPbI₃ [5, 9, 25, 26]. This process involves the formation of perovskite nanocrystals at a temperature of 115–129 °C, which gradually increase in size as the temperature is raised to 313–323 °C [9, 25, 26]. α -CsPbI₃ is a cubic black phase perovskite that can only be formed through annealing at a temperature above 300 °C. As the temperature decreases, this structure changes to the tetragonal black phase (β -CsPbI₃) at 260 °C, the orthorhombic black phase (γ -CsPbI₃) at 175 °C, and finally to the orthorhombic yellow phase (δ -CsPbI₃) at room temperature. The presence of PVP stabilizes the crystalline perovskite at room conditions [5, 6, 9, 13, 25, 26]. The exothermic peaks at 269 °C and 184 °C are likely due to the transitions from α to β and β to γ , respectively. The results of heating cycles show that as the concentration of polymer increases from 7.5% to 15%, the crystallinity of α -CsPbI₃ decreases from 84.4% to 24.0% (samples 1–4), and its stability at room temperature increases, as indicated by the cooling cycle. Although the highest crystallinity is observed at low polymer ratios (7.5% and 10%), high perovskite degradation occurs at 238 °C. Thus, XRD shows low crystallinity at low polymer concentrations at room temperature. Samples 3 and 4 exhibit high room temperature stability, with sample 3 having a higher perovskite crystallinity of 45.0%

Table 3 DSC results (cooling cycles)

	T ₄ , °C (midpoint)	ΔH_4 , J/g	T ₅ , °C (peak center)	ΔH_5 , J/g	T ₆ , °C (peak center)	ΔH_6 , J/g
1	270.2 ± 0.1	0.3	238.1 ± 2.8	16.4 ± 1.5	–	–
2	269.8 ± 0.1	0.3	240.1 ± 3.9	16.2 ± 0.2	–	–
3	268.2 ± 0.1	0.3	–	–	184.0 ± 0.5	0.2
4	269.2 ± 0.1	0.2	–	–	184.1 ± 0.6	0.2
5	271.0 ± 0.1	0.3	–	–	184.0 ± 0.1	0.2
6	270.8 ± 0.2 268.2 ± 0.1	0.3	–	–	183.7 ± 0.7	0.5

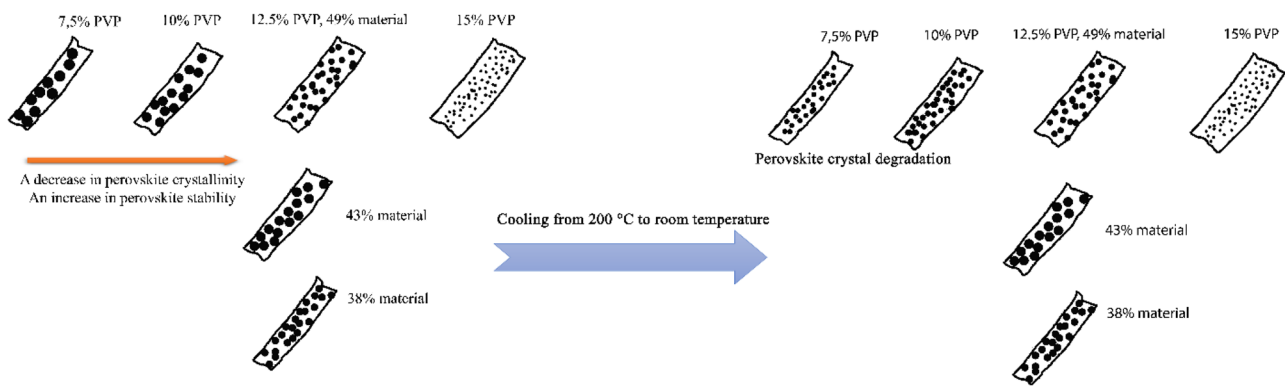


Fig. 4 A schematic illustration shows the difference in CsPbI₃ crystallinity at 200 °C (left part) and room temperature (right part)

compared to 24.0% in sample 4. Thus, XRD shows the best crystallinity for sample 3. As material concentration decreases, the crystallinity of perovskite increases from 45.0% at 49% material concentration to 83.8% at 43% material concentration and then slightly decreases to 78.7% at 38% material concentration. Figure 4 presents a schematic illustration that shows the difference in CsPbI₃ crystallinity at 200 °C and room temperature according to XRD and DSC results. A compromise between perovskite crystal size and stability is achieved at a polymer to perovskite ratio of 15% and a material concentration of 43% (sample 5).

Optical properties of nanofibers

The impact of solution concentration on the nanofibers optical properties was evaluated by recording light absorption and PL spectra. Figure 5a presents light absorption spectra of samples

1 to 6. Table 4 and Fig. S1 give the bandgap values of the samples. The light absorption spectrum covers most of the visible light region. Light absorption results agree with XRD results. The absorption intensity increases with increasing polymer concentration up to 12.5%, decreases at a PVP concentration of 15%, increases with decreasing material concentration from 49 to 43%, and decreases with a further decrease in the material concentration. This variation in light absorption is attributed to the change in perovskite crystallinity with manipulating polymer and material concentrations. The bandgap values vary between 1.72 eV and 1.74 eV. The optimal bandgap of 1.73 eV [5, 25] is obtained for samples 2, 3, 5, and 6. The PL spectra are shown in Fig. 5b. The PL intensity increases with increasing polymer concentration up to 12.5%, which is due to the passivating role of PVP in reducing crystalline defects. There is a slight decrease in PL intensity with increasing PVP concentration from 12.5% to 15%. The PL intensity does not change with lowering material concentration from 49 to 43%, but decreases with a further decrease up to 38%.

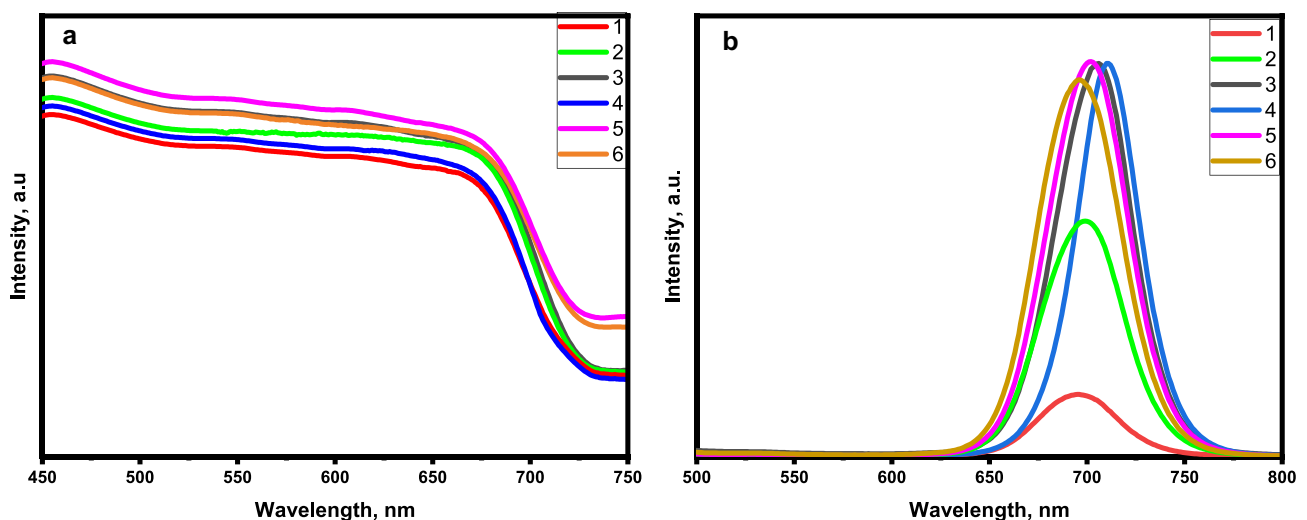


Fig. 5 Optical properties of nanofibers: **a** Light absorption spectra of samples (1–6); **b** PL spectra of samples (1–6)

Table 4 Bandgap values of samples 1–6

Sample	Optical bandgap, eV	Emission bandgap, eV(nm)
1	1.74	1.78(695)
2	1.73	1.77(699)
3	1.73	1.76(706)
4	1.74	1.74(711)
5	1.73	1.77(702)
6	1.73	1.78(696)

Table 4 gives the emission bandgap values of samples 1 to 6. A red shift is observed with increasing polymer concentration, and a blue shift is recorded with decreasing material concentration. The quantum effect and the structural constraints imposed by the polymer and nanofibrillar structure can explain these alterations [5, 6, 14, 28]. The optical bandgap values are lower than the values obtained from the PL spectra, which could be attributed to the transitions between direct and indirect band gaps [6].

The relationship between the average diameter and optical performance of nanofibers can be established based on the morphology and optical properties analysis of nanofibers. The polymer passivation and nano-sized crystals are responsible for crystalline perovskite stability under ambient conditions [5, 25, 26]. A larger diameter of nanofibers due to increased polymer concentration results in well-wrapped nanocrystals, increasing their stability over time. Conversely, a decrease in the diameter of nanofibers due to decreased material concentration leads to higher perovskite crystallinity but a decrease in its stability. Therefore, the average diameter should balance perovskite stability and crystallinity. However, with an average diameter of 329 nm, a material concentration of 43%, and a polymer to perovskite ratio of 15%, the ideal optical characteristics of nanofibers are reached.

Shrinkage after annealing

The shrinking of samples after annealing is a common occurrence in polymeric materials due to the polymer relaxation during heating. The stress of nanofibers during electrospinning explains this effect. The electrospinning process can lead to thermodynamically unstable stretched and oriented molecules, resulting in internal stress that can relax during annealing and cause significant shrinkage of electrospun nanofibers. The internal stress is caused by the solvent rapid evaporation during the electrospinning process due to the large surface area to volume ratio of nanofibers, the improved orientation and straightening by the rotary collector, and the increased mobility of polymer chains due

Table 5 Shrinkage ratio, solution concentration, and annealing temperature

	Sample direction	Shrinkage ratio, %
Perovskite concentration, %		
45.0% (Sample 3)	LD	12.4±0.7
	TD	14.7±0.5
40.3%	LD	15.8±2.2
	TD	17.6±4.0
35.1%	LD	28.2±0.5
	TD	30.7±0.5
Polymer concentration, %		
PVP, 12.5% (Sample 3)	LD	12.4±0.7
	TD	14.7±0.5
PVP, 15% (Sample 4)	LD	17.6±2.1
	TD	20.2±0.4
Material concentration, %		
49%, 488 nm (Sample 3)	LD	12.4±0.7
	TD	14.7±0.5
43%, 329 nm (Sample 5)	LD	13.4±0.3
	TD	14.3±0.4
38%, 228 nm (Sample 6)	LD	17.3±1.4
	TD	17.4±2.3
Annealing temperature, °C		
Sample 3–annealing at 200 °C for 5 min	LD	12.4±0.7
	TD	14.7±0.5
Sample 3–annealing at 150 °C for 5 min	LD	8.8±0.9
	TD	9.0±0.6

to the annealing process at a temperature above the T_g of the polymer [9, 29–32]. In our previous study [9], influence of the collector rotation speed on the nanofibers shrinkage ratio was investigated. The results showed that the shrinkage ratio increases with increasing the rotation speed due to the improved orientation and straightening of fibers. To have a better understanding of the mechanism of shrinking, the effect of solution concentration and annealing temperature on the shrinkage ratio was also studied. Nanofibers were collected using a rotary collector at a speed of 500 rpm, and the results are presented in Table 5.

The shrinkage in both LD and TD directions increases when perovskite concentration decreases because of increased polymer chain mobility [32], and when polymer concentration increases because of the increase in polymer fiber rigidity. The required relaxation time after electrospinning increases with more interlacing of polymer chains inside fibers with increasing polymer concentration [29]. Perovskite embedded in nanofibers controls the shrinkage of the polymer. Not only does the perovskite reduce the mobility of polymer chains, but it also helps to preserve the structure of samples (Fig. S2) [32]. The shrinkage ratio

also increases with decreasing material concentration due to the drop in the average diameter, leading to quicker solvent evaporation and higher stress [29], and decreases with decreasing annealing temperature due to a decrease in the mobility of polymer chains.

To control the deformation of electrospun nanofibers and decrease their shrinkage ratio, the following strategies can be used:

- Decreasing annealing temperature. Also, the nanofibers flexibility improves, but perovskite crystallinity and optical performance deteriorate [5];
- Increasing perovskite concentration. Furthermore, the nanofibers optical properties are improved [7, 11, 12], but simultaneously, a high increase in the average diameter and a drop in the nanofibers flexibility can be observed [5];
- Increasing material concentration (i.e., increasing the nanofibers average diameter). In addition, it leads to an increase in perovskite stability. However, this approach may negatively impact the nanofibers flexibility and perovskite crystallinity. Besides, a large increase in the average diameter can result in the shrinkage ratio increasing again due to the high stiffness and long relaxation time of nanofibers [29].
- Reducing polymer concentration. However, low polymer concentration (less than 12.5%, sample 3) will result in a high drop in the optical performance, tensile properties, and perovskite stability.

The shrinkage in the plane of nanofibers prepared on a substrate depends on the strength of the nanofiber's adhesion to the substrate [33, 34]. With a high enough weight of material deposited on a glass substrate (above 6.5 mg), empty edges, delamination, or cracks may be observed in samples (Fig. S3). This is due to the tensile stress that occurs in nanofibers after annealing as a result of the polymer shrinkage. Ways to reduce defects related to shrinkage include improving the nanofibers adhesion to the substrate, using substrates with a higher Young's modulus than that of the nanofibers, and making the nanofibers thickness smaller than that of the substrate [33, 34].

Tensile properties

The study of tensile properties of polymer-perovskite composite nanofibers is important for predicting and analyzing the behavior of optoelectronic devices under mechanical loads. The impact of solution concentration and annealing temperature on tensile properties of nanofibers were studied. The results are shown in Table 6 and Fig. 6. An increase in polymer concentration from 12.5% to 15%

leads to an improvement in strength from 0.8–1 MPa to 1–1.3 MPa, strain from 0.6–0.7% to 0.7–0.8%, and Young's modulus from 139–160 MPa to 157–169 MPa. It can be seen that the increase in the average diameter of nanofibers from 481 ± 122 nm to 558 ± 160 nm due to an increase in polymer concentration makes them more rigid and their elongation somewhat improves. As material concentration decreases from 49 to 43% (i.e., the nanofibers average diameter decreases from 481 ± 122 nm to 329 ± 70 nm), tensile properties improve from 0.8–1 MPa to 1.4–1.9 MPa strength, from 0.6–0.7% to 2.5–3.5% strain, and from 139–160 MPa to 79–112 MPa Young's modulus. As a result, nanofibers become stronger and more flexible. However, with a further decrease in material concentration from 43 to 38% (i.e., the nanofibers average diameter decreases from 329 ± 70 nm to 228 ± 51 nm), strength decreases from 1.4–1.9 MPa up to 0.9–1.2 MPa and strain from 2.5–3.5% to 1.1–1.2%, while Young's modulus changes slightly. Usually, tensile properties of polymer nanofibers improve by decreasing the average diameter owing to the improved molecular orientation and the drop in structural defects of nanofibers [35]. Nanocrystals formed in the polymer nanostructure (polymer to perovskite: 9–18%) lead to an increase in the number of weak points along the nanofibers, which becomes more significant as the average diameter greatly decreases (see Fig. 7). Thus, decreasing the concentration of these nanocrystals may lead to an improvement in the tensile properties. However, due to the annealing process and the shrinkage of the polymer, a lower concentration of perovskite results in sample deformation and an inability to determine the tensile properties (refer to Fig. S2). To understand the effect of the annealing process on the tensile properties of nanofibers, the tensile properties of unannealed nanofibers and those annealed at 200 °C and 150 °C for 5 min were determined. Before annealing, nanofibers consist of a complex composite. After annealing, nanocrystals are formed. These nanocrystals cause weak points to emerge, lowering the tensile properties of nanofibers (see Fig. 7). Smaller crystals are formed by decreasing the annealing temperature [5], resulting in enhanced tensile properties. Based on the discussion above, it can be concluded that the strength of nanofibers is mainly affected by the average diameter and annealing temperature, and the strain at break is mainly affected by the average diameter. By analyzing the results in Table 6, it can be seen that the highest tensile properties (strength of 1.9–1.4 MPa, strain of 3.5–2.5%) have been recorded for a polymer to perovskite ratio of 15% and a material concentration of 43%. However, they can be further enhanced by increasing the ratio of polymer to perovskite or/and by decreasing the annealing temperature, but this will reduce the optical performance of nanofibers. Thus, solution 5 (a polymer to perovskite ratio of 15% and a material concentration of 43%) achieves a compromise between the tensile and optical properties of nanofibers.

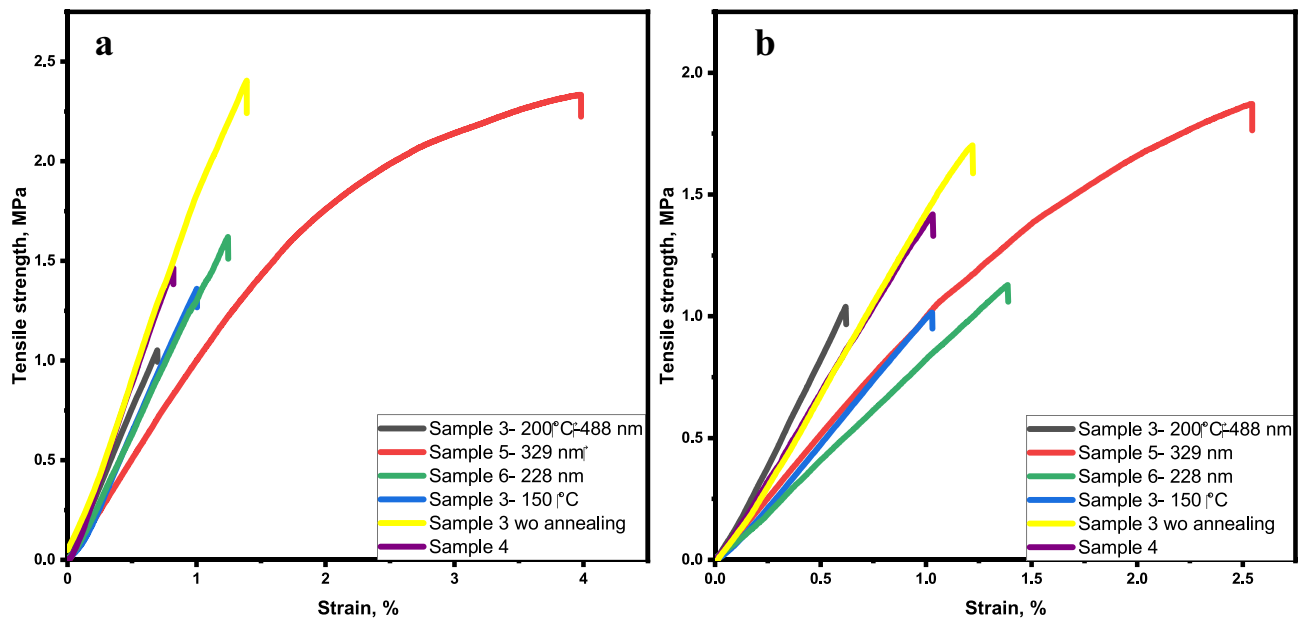
Tab 6 Tensile properties, solution concentration, and annealing temperature

	LD/ TD	Strain at break, %	Tensile strength, MPa	Young's Modulus, MPa
Polymer concentration, %				
Sample 3–12.5% PVP	LD	0.7±0.1	1.0±0.1	160.3±26.3
	TD	0.6±0.1	0.8±0.2	139.0±33.4
Sample 4–15% PVP	LD	0.8±0.1	1.3±0.1	169.0±26.9
	TD	0.7±0.1	1.0±0.3	157.4±40.6
Material concentration, %				
49%, 488 nm (Sample 3)	LD	0.7±0.1	1.0±0.1	160.3±26.3
	TD	0.6±0.1	0.8±0.2	139.0±33.4
43%, 329 nm (Sample 5)	LD	3.5±1.0	1.9±0.4	112.3±14.6
	TD	2.5±0.1	1.4±0.4	79.2±25.4
38%, 228 nm (Sample 6)	LD	1.2±0.4	1.2±0.3	111.8±43.7
	TD	1.1±0.3	0.9±0.2	93.8±9.8
Annealing temperature, °C				
Sample 3–200 °C	LD	0.7±0.1	1.0±0.1	160.3±26.3
	TD	0.6±0.1	0.8±0.2	139.0±33.4
Sample 3–150 °C	LD	1.0±0.2	1.1±0.2	133.5±15.1
	TD	0.8±0.2	0.8±0.2	111.9±11.3
Sample 3– without annealing	LD	1.2±0.1	1.9±0.3	185.4±9.0
	TD	0.9±0.1	1.5±0.2	174.4±27.1

In comparison to the tensile properties of PVP nanofibers [36–38] or PVP composite nanofibers (strain: 10–30%, tensile strength: 1–8 MPa) [39, 40], the tensile properties of the obtained nanofibers in this work must be improved to be suitable for flexible optoelectronic devices.

Thermal stability of nanofibers

A study was done using TGA to determine the effect of solution concentration on thermal properties of nanofibers. The analysis results of samples (PVP powder, PVP nanofibers, 1,

**Fig. 6** Tensile strength–strain diagrams of samples with maximum strength in LD (a) and in TD (b)

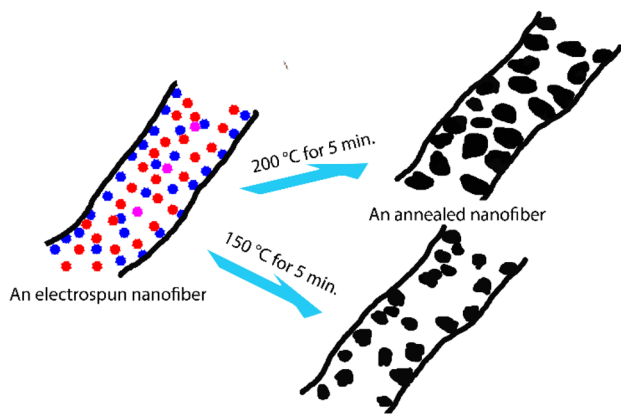


Fig. 7 An illustration of the structure of nanofibers before and after annealing at 150 °C and 200 °C for 5 min

3, and 5) are shown in Fig. 8 and Table 7. It can be noticed that composite nanofibers exhibit higher thermal stability than PVP powder or nanofibers due to the embedded perovskite. At a temperature of 200 °C, they lose 1.8–3.6% of their weight. A noticeable weight loss of samples with perovskite is observed around a temperature of 135 °C, which indicates the solvent full evaporation. It is also seen that PVP nanofibers exhibit lower thermal stability than PVP powder, which is consistent with other results reported in the literature [41]. This can be attributed to the following reasons:

PVP nanofibers contain solvent residues and have a higher moisture content than powder. Thus, the weight loss of nanofibers is greater than that of powder;

The large surface area to volume ratio of nanofibers increases the heat transfer surface, making nanofibers more susceptible to thermal degradation [42];

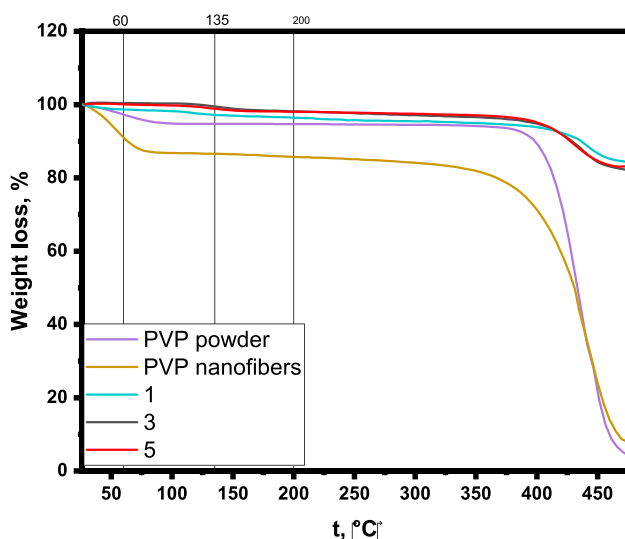


Fig. 8 TGA analysis of nanofibers

Table 7 TGA results

	PVP powder	PVP nanofibers	1	3	5
Extrapolated onset temperature, °C	396.4	371.5	419.8	398.8	402.4
Weight loss, % 200 °C	90.5	79.3	92.4	94.9	94.8
Weight loss, %	94.7	85.7	96.4	98.1	98.0

The strain in polymer nanofibers after electrospinning could affect their thermal stability [29, 31, 43].

Actually, thermal properties of polymer nanofibers are affected by a variety of factors, including the polymer type [41, 43–46], the crystallinity degree of the polymer and the aligned structure after electrospinning [43], and the solvents used [47]. Therefore, it is difficult to predict.

Conclusion

The quality of PVP:CsPbI₃ nanofibers (i.e., morphology, crystallinity, optical properties, shrinkage ratio, tensile properties, thermal stability) was improved by manipulating the electrospinning solution concentration. The solution concentration should balance perovskite stability and crystallinity. Increasing polymer concentration up to 12.5% (polymer:perovskite, 15:85) led to an enhancement in perovskite crystallinity and optical properties because of the increase in perovskite stability, while decreasing material concentration up to 43% (for the same polymer to perovskite ratio of 15%) led to a further increase in the crystallinity and optical properties due to the decrease in the confinement effect of the polymer. The optimal bandgap energy value of 1.73 eV is achieved at a polymer concentration of 10–12.5% and a material concentration of 43–38%. The electrospinning solution (a polymer to perovskite ratio of 15%, a material concentration of 43%) achieved a compromise between optical performance and tensile properties of nanofibers. The tensile properties of nanofibers can be even more improved by increasing polymer concentration, but this leads to a decrease in perovskite crystallinity. The shrinkage mechanism of the composite nanofibers was determined. The shrinkage can be reduced by increasing the average diameter, i.e., increasing the material or perovskite concentrations. However, these methods can result in a drop in the optical performance or the flexibility of nanofibers, respectively. Despite the fact that the decrease in the annealing temperature can lead to a decrease in the shrinkage ratio and an increase in tensile properties, it results in a high drop in perovskite crystallinity and optical properties. The perovskite included into the polymer nanofibers helps to reduce

shrinkage and prevent deformation during the annealing process. Proper control of the thickness and Young's modulus of both the nanofibers and the substrate is crucial to achieve compatibility between them. The results of the work could help to accelerate the development of polymer-perovskite nanocomposites and devices based on them.

Supplementary Information The online version contains supplementary material available at <https://doi.org/10.1007/s10965-023-03578-w>.

Author contributions The authors contributed equally to this work.

Declarations

Conflicts of interest The authors declare that they have no conflict of interest.

References

- Shalan AE, Barhoum A, Elseman AM, Rashad MM, Lira-Cantú M (2018) Nanofibers as promising materials for new generations of solar cells. *Handbook of Nanofibers*, Springer International Publishing, Cham 1–33. https://doi.org/10.1007/978-3-319-42789-8_51-1
- Bkkar M, Olekhovich R, Uspenskaya M (2020) Obtaining nanofibers based on perovskite-polymer composites for applying in solar cells. *International Multidisciplinary Scientific GeoConference Surveying Geology and Mining Ecology Management, SGEM 20:129–136*. <https://doi.org/10.5593/sgem2020/4.1/s17.017>
- Cao B, Yang L, Jiang S, Lin H, Wang N, Li X (2019) Flexible quintuple cation perovskite solar cells with high efficiency. *J Mater Chem A* 7:4960–4970. <https://doi.org/10.1039/c8ta11945g>
- Wang Y, Yokota T, Someya T (2021) Electrospun nanofiber-based soft electronics. *NPG Asia Mater* 13:22. <https://doi.org/10.1038/s41427-020-00267-8>
- Bkkar MA, Olekhovich RO, Kremleva AV, Kovach YN, Kalanchina V, Uspenskaya MV (2022) Fabrication of electrospun polymer nanofibers modified with all-inorganic perovskite nanocrystals for flexible optoelectronic devices. *Appl Nanosci* 12:2961–2977. <https://doi.org/10.1007/s13204-022-02603-6>
- Bohr C, Pfeiffer M, Öz S, von Toperczer F, Lepcha A, Fischer T, Mathur S (2019) Electrospun hybrid perovskite fibers-flexible networks of one-dimensional semiconductors for light-harvesting applications. *ACS Appl Mater Interfaces* 11:25163–25169. <https://doi.org/10.1021/acsami.9b05700>
- Li G, Jiang Z, Wang W, Chu Z, Zhang Y, Wang C (2019) Electrospun PAN/MAPBI₃ composite fibers for flexible and broadband photodetectors. *Nanomaterials* 9:50. <https://doi.org/10.3390/nano9010050>
- Chen L, Chuang Y, Yang WD, Tsai K C, Chen CW, Dong CD (2021) All-inorganic perovskite CsPbX₃ electrospun nanofibers with color-tunable photoluminescence and high performance optoelectronic applications. *J Alloys Compd* 856:157426. <https://doi.org/10.1016/j.jallcom.2020.157426>
- Bkkar M, Olekhovich R, Kremleva A, Sitnikova V, Kovach Y, Zverkov N, Uspenskaya M (2023) Influence of electrospinning setup parameters on properties of polymer-perovskite nanofibers. *Polymers (Basel)* 15:731. <https://doi.org/10.3390/polym15030731>
- Zhang H, Fu D, Du Z, Fu H, Shao G, Yang W, Zheng J (2020) In situ growth of aligned CsPbBr₃ nanorods in polymer fibers with tailored aspect ratios. *Ceram Int* 46:18352–18357. <https://doi.org/10.1016/j.ceramint.2020.04.035>
- Meng L, Yang C, Meng J, Wang Y, Ge Y, Shao Z, Zhong H (2019) In-situ fabricated anisotropic halide perovskite nanocrystals in polyvinylalcohol nanofibers: shape tuning and polarized emission. *Nano Res* 12:1411–1416. <https://doi.org/10.1007/s12274-019-2353-4>
- Yang M, Yu J, Jiang S, Zhang C, Sun Q, Wang M, Lei F (2018) High stability luminophores: fluorescent CsPbX₃ (X = Cl, Br and I) nanofiber prepared by one-step electrospinning method. *Opt Express* 26:20649. <https://doi.org/10.1364/oe.26.020649>
- Ercan E, Tsai PC, Chen JY, Lam JY, Hsu LC, Chueh CC, Chen WC (2019) Stretchable and ambient stable perovskite/polymer luminous hybrid nanofibers of multicolor fiber mats and their white LED applications. *ACS Appl Mater Interfaces* 11:23605–23615. <https://doi.org/10.1021/acsami.9b05527>
- Chen Y, Zhang S, Wang J (2020) Electrospinning of perovskite crystals with strong emission and improved electrical conductivity. *International Conference on Artificial Intelligence and Electromechanical Automation (AIEA)*, IEEE 715–719. <https://doi.org/10.1109/AIEA51086.2020.00159>
- Ünlü F, Jung E, Haddad J, Kulkarni A, Öz S, Choi H, Fischer T, Chakraborty S, Kirchartz T, Mathur S (2020) Understanding the interplay of stability and efficiency in A-site engineered lead halide perovskites. *APL Mater* 8. <https://doi.org/10.1063/5.0011851>
- Boyd CC, Cheacharoen R, Leijtens T, McGehee MD (2019) Understanding degradation mechanisms and improving stability of perovskite photovoltaics. *Chem Rev* 119:3418–3451. <https://doi.org/10.1021/acs.chemrev.8b00336>
- Bartel CJ, Sutton C, Goldsmith BR, Ouyang R, Musgrave CB, Ghiringhelli LM, Scheffler M (2019) New tolerance factor to predict the stability of perovskite oxides and halides. *Sci Adv* 5:1–9. <https://doi.org/10.1126/sciadv.aav0693>
- Fiscicaro G, La Magna A, Alberti A, Smecca E, Mannino G, Deretzis I (2020) Local order and rotational dynamics in mixed A-cation lead iodide perovskites. *J Phys Chem Lett* 11:1068–1074. <https://doi.org/10.1021/acs.jpcclett.9b03763>
- Ghosh D, Smith AR, Walker AB, Islam MS (2018) Mixed A-cation perovskites for solar cells: atomic-scale insights into structural distortion, hydrogen bonding, and electronic properties. *Chem Mater* 30:5194–5204. <https://doi.org/10.1021/acs.chemmater.8b01851>
- Li B, Fu L, Li S, Li H, Pan L, Wang L, Yin L (2019) Pathways toward high-performance inorganic perovskite solar cells: Challenges and strategies. *J Mater Chem A* 7:20494–20518. <https://doi.org/10.1039/c9ta04114a>
- Li Z, Yang M, Park JS, Wei SH, Berry JJ, Zhu K (2016) Stabilizing perovskite structures by tuning tolerance factor: formation of formamidinium and cesium lead iodide solid-state alloys. *Chem Mater* 28:284–292. <https://doi.org/10.1021/acs.chemmater.5b04107>
- Miyasaka T, Kulkarni A, Kim GM, Öz S, Jena AK (2020) Perovskite solar cells: can we go organic-free, lead-free, and dopant-free? *Adv Energy Mater* 10. <https://doi.org/10.1002/aenm.201902500>
- Romiluyi O, Eatmon Y, Ni R, Rand BP, Clancy P (2021) The efficacy of Lewis affinity scale metrics to represent solvent interactions with reagent salts in all-inorganic metal halide perovskite solutions. *J Mater Chem A* 9:13087–13099. <https://doi.org/10.1039/d1ta3a>
- Kirakosyan A, Kim Y, Sihn MR, Jeon MG, Jeong JR, Choi J (2020) Solubility-controlled room-temperature synthesis of cesium lead halide perovskite nanocrystals. *ChemNanoMat* 6:1863–1869. <https://doi.org/10.1002/cnma.202000471>
- Li B, Zhang Y, Fu L, Yu T, Zhou S, Zhang L, Yin L (2018) Surface passivation engineering strategy to fully-inorganic cubic CsPbI₃ perovskites for high-performance solar cells. *Nat Commun* 9:1–8. <https://doi.org/10.1038/s41467-018-03169-0>
- Ye T, Zhou B, Zhan F, Yuan F, Ramakrishna S, Golberg D, Wang X (2020) Below 200 °C Fabrication strategy of black-phase CsPbI₃ film for ambient-air-stable solar cells. *Sol RRL* 4:1–9. <https://doi.org/10.1002/solr.202000014>
- Wang B, Novendra N, Navrotsky A (2019) Energetics, structures, and phase transitions of cubic and orthorhombic cesium lead

- iodide (CsPbI₃) polymorphs. *J Am Chem Soc* 141:14501–14504. <https://doi.org/10.1021/jacs.9b05924>
28. Tsai PC, Chen JY, Ercan E, Chueh CC, Tung SH, Chen WC (2018) Uniform luminous perovskite nanofibers with color-tunability and improved stability prepared by one-step core/shell electrospinning. *Small* 14:1–9. <https://doi.org/10.1002/sml.201704379>
 29. Elishav O, Beilin V, Rozent O, Shter GE, Grader GS (2018) Thermal shrinkage of electrospun PVP nanofibers. *J Polym Sci Part B Polym Phys* 56:248–254. <https://doi.org/10.1002/polb.24538>
 30. Liu L, Li T, Sun M, Jia W, Jiao K, Wang S, Luo Y (2022) Preparation of temperature-controlled shrinkage PTMC/PVP core-shell nanofibrous membrane with spindle-knotted structure for accelerating wound closure. *Mater Lett* 324:132601. <https://doi.org/10.1016/j.matlet.2022.132601>
 31. Fang F, Wang H, Wang H, Huang WM, Chen Y, Cai N, Chen X (2021) Stimulus-responsive shrinkage in electrospun membranes: Fundamentals and control. *Micromachines* 12:1–10. <https://doi.org/10.3390/mi12080920>
 32. Rozent O, Beilin VV, Shter GE, Grader GS (2016) Deformation control during thermal treatment of electrospun PbZr_{0.52}Ti_{0.48}O₃ nanofiber mats. *J Am Ceram Soc* 99:1550–1556. <https://doi.org/10.1111/jace.14203>
 33. Tirumkudulu MS, Punati VS (2022) Solventborne Polymer coatings: drying, film formation, stress evolution, and failure. *Langmuir* 38:2409–2414. <https://doi.org/10.1021/acs.langmuir.1c03124>
 34. Lei H, Francis LF, Gerberich WW, Scriven LE (2002) Stress development in drying coatings after solidification. *AIChE J* 48:437–451. <https://doi.org/10.1002/aic.690480304>
 35. Wong SC, Baji A, Leng S (2008) Effect of fiber diameter on tensile properties of electrospun poly(ϵ -caprolactone). *Polymer (Guildf)* 49:4713–4722. <https://doi.org/10.1016/j.polymer.2008.08.022>
 36. Doderio A, Brunengo E, Castellano M, Vicini S (2020) Investigation of the mechanical and dynamic-mechanical properties of electrospun polyvinylpyrrolidone membranes: a design of experiment approach. *Polymers (Basel)* 12:1524. <https://doi.org/10.3390/polym12071524>
 37. Huang S, Zhou L, Li M-C, Wu Q, Kojima Y, Zhou D (2016) Preparation and properties of electrospun poly (vinyl pyrrolidone)/cellulose nanocrystal/silver nanoparticle composite fibers. *Materials (Basel)* 9:523. <https://doi.org/10.3390/ma9070523>
 38. Ghelich R, Jahannama MR, Abdizadeh H, Torknik FS, Vaezi MR (2022) Effects of hafnium and boron on antibacterial and mechanical properties of polyvinylpyrrolidone-based nanofibrous composites. *Polym Bull* 79:5885–5899. <https://doi.org/10.1007/s00289-021-03627-8>
 39. Hashmi M, Ullah S, Ullah A, Saito Y, Haider MK, Bie X, Wada K, Kim IS (2021) Carboxymethyl cellulose (CMC) based electrospun composite nanofiber mats for food packaging. *Polymers (Basel)* 13:1–12. <https://doi.org/10.3390/polym13020302>
 40. Rahmani F, Ziyadi H, Baghali M et al (2021) Electrospun PVP/PVA nanofiber mat as a novel potential transdermal drug-delivery system for buprenorphine: A solution needed for pain management. *Appl Sci* 11. <https://doi.org/10.3390/app11062779>
 41. Kim WT, Park DC, Yang WH, Cho CH, Choi WY (2021) Effects of electrospinning parameters on the microstructure of PVP/TiO₂ nanofibers. *Nanomaterials* 11:26–28. <https://doi.org/10.3390/nano11061616>
 42. Mottin AC, Ayres E, Oréface RL, Câmara JJD (2016) What changes in poly(3-hydroxybutyrate) (PHB) when processed as electrospun nanofibers or thermo-compression molded film? *Mater Res* 19:57–66. <https://doi.org/10.1590/1980-5373-MR-2015-0280>
 43. Carrizales C, Pelfrey S, Rincon R, Eubanks TM, Kuang A, McClure MJ, Bowlin GL, Macosay J (2008) Thermal and mechanical properties of electrospun PMMA, PVC, Nylon 6, and Nylon 6,6. *Polym Adv Technol* 19:124–130. <https://doi.org/10.1002/pat.981>
 44. Neisiany RE, Khorasani SN, Lee YKJ, Ramakrishna S (2016) Encapsulation of epoxy and amine curing agent in PAN nanofibers by coaxial electrospinning for self-healing purposes. *RSC Adv* 6:70056–70063. <https://doi.org/10.1039/C6RA06434E>
 45. El-Newehy MH, Al-Deyab SS, Kenawy E-R, Abdel-Megeed A (2012) Fabrication of electrospun antimicrobial nanofibers containing metronidazole using nanospider technology. *Fibers Polym* 13:709–717. <https://doi.org/10.1007/s12221-012-0709-4>
 46. Xu W-C, Zhong L-B, Shao Z-D, Dou S, Yu L, Cheng X, Zheng YM (2021) Rational design of pore structures for carbon aerogels to significantly increase adsorption of tetracycline from water using batch and fixed-bed operation. *Environ Sci Nano* 8:3250–3261. <https://doi.org/10.1039/D1EN00459J>
 47. Xu Y, Zou L, Lu H, Kang T (2017) Effect of different solvent systems on PHBV/PEO electrospun fibers. *RSC Adv* 7:4000–4010. <https://doi.org/10.1039/C6RA26783A>

Publisher's Note Springer Nature remains neutral with regard to jurisdictional claims in published maps and institutional affiliations.

Springer Nature or its licensor (e.g. a society or other partner) holds exclusive rights to this article under a publishing agreement with the author(s) or other rightsholder(s); author self-archiving of the accepted manuscript version of this article is solely governed by the terms of such publishing agreement and applicable law.